Applied Organometallic Chemistry **WILEY**

# Readily accessible mesoporous silica nanoparticles supported chiral urea-amine bifunctional catalysts for enantioselective reactions

Yaşar Gök [ID] | İrem Tutkum Aykut | Halil Zeki Gök [ID]

Department of Biomedical Engineering, Bucak Faculty of Technology, Burdur Mehmet Akif Ersoy University, Burdur, Turkey

**Correspondence**
Halil Zeki Gök, Department of Biomedical Engineering, Bucak Faculty of Technology, Burdur Mehmet Akif Ersoy University, Bucak, Burdur 15300, Turkey.
Email: zekigok@mehmetakif.edu.tr; yasargok@mehmetakif.edu.tr

The main objective of this study is to develop readily accessible and recyclable solid catalysts for enantioselective reactions. To achieve this, magnetic MCM-41 and non-magnetic SBA-15 mesoporous supports were prepared, then mesoporous silica supported chiral urea-amine bifunctional catalysts were synthesized by grafting of chiral urea-amine ligand onto SBA-15 and magnetic MCM-41. The magnetic and non-magnetic supports and so-prepared solid catalysts were characterized by using different methods such as $N_2$ sorption measurements, Fourier transform infrared spectroscopy (FT-IR), field emission scanning electron microscope-energy dispersive X-ray analysis (FESEM-EDX), X-ray diffraction (XRD), and thermogravimetric analysis (TGA). Results showed that (1*R*, 2*R*) or (1*S*, 2*S*)-1,2-diphenylethane-1,2-diamine was successively immobilized onto magnetic MCM-41 and SBA-15 pores. The heterogeneous chiral solid catalysts and their homogenous counterparts exhibited high activities both enantioselective transfer hydrogenation reaction (up to 99% conversion and 65% *ee*) and enantioselective Michael reaction (up to 98% conversion and 26% *ee*). Moreover, the SBA-15 supported solid catalysts were separated from the reaction mixture by simple filtration, whereas the magnetic MCM-41 supported solid catalysts were separated by simple magnetic decantation and reused in three consecutive catalytic experiments.

**KEYWORDS**
chirality, enantioselectivity, heterogeneous catalysis, mesoporous materials

## 1 | INTRODUCTION

The vast majority of modern medicines and pesticides used today contain the only one type of stereoisomeric structure of the chemical substance. One of the enantiomers contained in pure nonstereoisomer drugs has the desired effect for the organism, whereas the other enantiomer may have negative effects.[1,2] Thalidomide is a nausea remedy used in the 1950s. However, one of the enantiomers contained in racemic thalidomide helps to relieve nausea, whereas the other enantiomer has been shown to have negative effects on the fetus. After this tragedy, the research on the active ingredients of modern drugs has begun to be the only one enantiomer.[3–6]

Homogeneous enantioselective catalysis is a very powerful method used in the preparation of chiral molecules for modern drugs. Prochiral starting compounds can be converted into chiral products as a result of the reaction catalyzed by a small amount of a chiral ligand in enantioselective catalysis.[7–9] To date, a large number of chiral catalysts with very high catalytic activity for enantioselective catalysis has been published in the

literature.[10–15] However, the industrial applications of these privileged stereodirecting chiral catalysts are often hindered by their high costs, the inability to recover them after their use, and the removal of these toxic metals from the organic product. Many different approaches have been tried to facilitate easy recovery and recycling of highly selective chiral catalysts. One of these approaches is the fixation of the homogeneous chiral catalyst by attaching it to a support material.[16–19] SBA- and MCM-type silicas are two of the most popular support materials used in the fixation of chiral catalyst via covalent bond due to their ordered structure, very high surface areas, uniform, tunable pore size, chemical composition, shapes, and surface properties.[20–26] Silyl derivatives of active catalysts can be grafted to the walls of silica supports by condensation of organosilane derivative of catalysts with Si-OH groups on the surface of support materials. Prepared heterogeneous materials for the enantioselective catalysis have the advantages of the simplicity of removal, regeneration, and reusability of them.[27,28] In most cases, the removal of solid catalyst can be performed by a simple filtration or centrifugation. However, in some cases, recovering of solid catalyst from reaction mixture could not be possible by these techniques. Thanks to the magnetic nanoparticles. Magnetic nanoparticles can be coated by silica shell and thus, formed core-shell composite material has the benefits of magnetic properties with the physicochemical properties of silica. By using an external magnet, the solid catalyst on magnetic support can be recycled easily by magnetic decantation.[29–32] Therefore, preparation of solid catalysts on magnetic support have attracted much attention due to their great advantages in separation, purification, and recycling and gained interest for application in biodiesel production,[29,30] preparation of chiral and non-chiral molecules,[33–35] drug delivery,[36,37] cancer therapy,[38,39] and theranostic applications.[40]

Chiral catalysts with many different functional groups on different type of supports have been synthesized so far to be used in enantioselective catalysis.[41–48] However, many newly synthesized heterogeneous catalysts show low catalytic activity. In recent years, it has come to the fore to obtain suitable heterogeneous catalysts by grafting of known highly effective homogeneous chiral catalysts to mesoporous silica nanoparticles instead of the synthesis of new chiral ligands. Privileged chiral ligands are known as efficient homogenous catalysts. Chiral ligands with $C_2$ symmetry are known as privileged chiral catalysts that give very good results in homogeneous enantioselective catalysis.[49,50] The common point of $C_2$ symmetric chiral ligands is that they have the rigid structure containing functional groups with donor atoms such as oxygen, nitrogen, and phosphorous which allow the chiral ligand to coordinate to the metal atom. (1R, 2R) or (1S, 2S)-1,-2-diphenylethane-1,2-diamine as a member of $C_2$ symmetric ligands and has been subject of many studies in the field of enantioselective catalysis.[51–54] However, the studies in enantioselective heterogeneous catalysis with the immobilized 1,2-diphenylethane-1,2-diamine onto the mesoporous materials are still limited.

On account of given explanation above, in this study, initially SBA-15 and magnetic MCM-41 were prepared as supporting material. Then, silyl derivatives of (1R, 2R) or (1S, 2S)-1,2-diphenylethane-1,2-diamine 4 and 5 were synthesized by the reaction of (1R, 2R) or (1S, 2S)-1,2-diphenylethane-1,2-diamine with triethoxy(3-isocyanatopropyl)silane. Thereafter organofunctionalized silica nanoparticles were prepared by the condensation of terminal organosilane of 4 and 5 with the Si—OH groups on the surface of silica supports. The catalytic efficiency of prepared heterogeneous catalysts was tested in enantioselective transfer hydrogenation and enantioselective Michael reaction. The effect of different morphology and pore size in the case of SBA-15 and magnetic MCM-41 on the catalytic performance in asymmetric catalysis was also investigated. The novelty of the present research is the easy preparation of heterogeneous solid catalyst on magnetic and non-magnetic silica support in different morphology and pore size and their application in different type of enantioselective heterogeneous catalysis.

## 2 | EXPERIMENTAL

### 2.1 | Materials and equipment

Pluronic P123, triethoxy(3-isocyanatopropyl)silane (IPTES), cetyltrimethylammonium bromide (CTAB), tetraethyl orthosilicate (TEOS), (1R, 2R)-1,2-diphenylethane-1,2-diamine, (1S, 2S)-1,2-diphenylethane-1,2-diamine, and all other reagents were obtained from commercial suppliers (Merck or Fluka). All the materials used during the experiments were of analytical grade. Drying and purification of solvents used in this study were performed by following the procedure in Perrin and Armarego.[55] Infrared spectroscopy was performed using Fourier transform infrared spectroscopy (FT-IR), the spectrum 65 Fourier infrared spectrometer from Perkin Elmer using KBr pellet technique. Nuclear magnetic resonance (NMR) measurements for $^1$H and $^{13}$C were acquired in CDCl$_3$ on a Bruker AVANCE III 400 MHz NaNoBay. Liquid chromatography with tandem mass spectrometry (LC–MS/MS) measurements were recorded on an Agilent LC–MS/MS 6460 Triple Quad, whereas a Bruker Daltonics spectrometer was used

for matrix assisted laser desorption ionization-time of flight (MALDI-TOF) measurements. The X-ray diffraction (XRD) measurement was carried out on a PANalytical Empyrean X-ray diffractometer using Cu-Kα radiation ($\lambda = 0.154056$ nm) within the scattering angle $2\theta$ range of $1°–10°$, and $10°–80°$, respectively. Jeol SEM-7100-EDX instrument was used to record the field emission scanning electron microscope (FESEM) images of samples. The thermogravimetric analysis (TGA) measurements were carried out on a Seiko SII TG/DTA 7200 instrument. The flow rate of $N_2$ gas was 2 ml min$^{-1}$ and the rate of heat was 10°C min$^{-1}$ during the TGA analysis. $N_2$ sorption isotherms were recorded on a Micrometrics Surface Area and Porosity Tristar II analyzer. Brunauer–Emmett–Teller (BET) method was used to calculate the surface area of mesoporous materials, whereas Barrett, Joyner, and Halenda (BJH) method was used for the calculation of pore size distribution. The measurements of optical activity of products was recorded in a Rudolph Autopol I polarimeter. Stuart SMP10 electrothermal equipment were used to determine the melting points. Enantiomeric excess was determined on a Shimadzu Prominence LC-20A with DAD detection using YMC Chiral ART Amylose-C column and on Shimadzu GC-2010 Plus using chiral column (HP-Chiral-20B).

## 2.2 | Synthesis

### 2.2.1 | Synthesis of SBA-15

The synthesis of SBA-15 was performed by following the previously published procedure.[56] The gel composition of TEOS:P123:HCl:$H_2O$ was 1.00:0.02:5.58:182.55, respectively. Briefly, Pluronic P123 (16 g) was placed in a flask containing 1.6 M HCl (600 ml) under stirring at 41°C. After Pluronic P123 was dissolved, to the solution was added TEOS (37 ml) dropwise. Then, the temperature reduced to 25°C and kept stirring for further 20 h followed by aging at 80°C for 15 h. Separation of the gel portion by filtration, then washing with water and ethyl alcohol afforded the white precipitate. The precipitate was dried in oven at 60°C for overnight. Calcination at 550°C for 8 h to remove the template yielded the final mesoporous SBA-15 nanoparticles.

### 2.2.2 | Synthesis of $Fe_3O_4$

The coprecipitation method was applied for the synthesis of $Fe_3O_4$ nanoparticles.[57] For this, $FeCl_3.6H_2O$ (8.5 g; 52.6 mmol), $FeCl_2.4H_2O$ (2.26 g; 17.9 mmol) were put together in a flask and dissolved by adding deionized

water (402 ml). The temperature of the stirring reaction content was raised to 80°C. At this temperature, ammonia solution was added dropwise to the reaction content and stirred for a further 2 h at 80°C. After 2 h, the temperature was allowed to cool to 25°C and then decanted with the help of external magnet. The magnetic nanoparticles were washed with water till they were neutral. Drying the precipitant in an oven at 80°C for 4 h, then under vacuum at 70°C for further 12 h afforded the desired product $Fe_3O_4$.

### 2.2.3 | Synthesis of $Fe_3O_4$@MCM-41 (mMCM-41)

$Fe_3O_4$ nanoparticles (0.39 g; 1.7 mmol) were dispersed in 600 ml of deionized water by using an ultrasonic bath for 10 min. CTAB (3.12 g) was then added to the solution containing $Fe_3O_4$ nanoparticles, and temperature was raised up to 70°C. After stirring 30 min, to the reaction mixture was added TEOS (15 ml) over a 1 h period. The temperature of reaction was allowed to cool to 25°C and stirred for further 3 h. Ammonia solution (25%) was added until the reaction pH was 10 and stirred for another 12 h. The gel portion was separated by filtration. It was then washed with water and ethyl alcohol. The precipitate was dried in oven at 120°C for 2 h. Removing of template was carried out by calcination at 450°C for 4 h, yielding the final mesoporous mMCM-41 nanoparticles.[58]

### 2.2.4 | 1-((1R,2R)-2-amino-1,2-diphenylethyl)-3-(3-(triethoxysilyl)propyl)urea (4)

A solution of triethoxy(3-isocyanatopropyl)silane **1** (0.113 g, 0.43 mmol) in dry DCM (6 ml) was added over 1 h to the solution of (R, R) enantiomer of diamine **2** (0.1 g, 0.47 mmol) in dry DCM (4 ml) under inert atmosphere at 25°C. Formation of products and depletion of reactants were followed by TLC. After 24 h, the reaction mixture was transferred into an evaporator flask, and the solvent of the reaction mixture was evaporated under reduced pressure. The remaining crude product was subjected to the silica gel column chromatography. The solvent system was DCM:MeOH (97:3), affording pure **4** as a transparent oil. Yield: 0.13 g (66%). Found: C, 62.28; H, 7.98; N, 9.01%; "molecular formula $C_{24}H_{37}N_3O_4Si$" requires C, 62.71; H, 8.11; N, 9.14%. $[\alpha]_D^{20} = +11$ (c, 1.0, CHCl$_3$). FT-IR (disk) $\nu = 3,317$, 3,065, 3,028, 3,006, 2,974, 2,925, 1,632, 1,559, 1,494, 1,453, 1,390, 1,242, 1,216, 1,193, 1,165, 1,100, 1,073, 1,029,

954 cm$^{-1}$. $^1$H-NMR (400 MHz, CDCl$_3$, ppm) $\delta$: 0.43–0.47 (m, 2H), 1.14 (t, $J$ = 7.0 Hz, 9H), 1.41–1.46 (m, 2H), 1.92–2.04 (br, s, 2H), 2.98–3.03 (m, 2H), 3.71 (q, $J$ = 7.0 Hz, 6H), 4.53–4.56 (m, 1H), 5.65–5.67 (m, 1H), 7.03–7.06 (m, 2H), 7.13–7.18 (m, 3H), 7.20–7.25 (m, 7H). $^{13}$C-NMR (100 MHz, CDCl$_3$, ppm) $\delta$: 7.5 (CH$_2$), 18.2 (CH$_3$), 23.4 (CH$_2$), 42.9 (CH$_2$), 58.4 (CH$_2$), 60.2 (CH), 60.4 (CH), 126.6 (CH), 126.7 (CH), 127.3 (CH), 127.4 (CH), 128.4 (CH), 128.5 (CH), 141.2 (C), 142.3 (C), 157.9 (C). MS (ESI$^+$) MS calculated [M + H]$^-$ for C$_{24}$H$_{38}$N$_3$O$_4$Si: 460.2 found: 460.20 [M + H]$^+$.

## 2.2.5 | 1-((1S,2S)-2-amino-1,2-diphenylethyl)-3-(3-(triethoxysilyl)propyl)urea (5)

To obtain (S, S) derivative **5**, the above-mentioned procedure was carried out except (S, S) diamine derivative **3** used instead of **1**. C$_{24}$H$_{37}$N$_3$O$_4$Si **5**. Yield: 68%. Found: C, 62.52; H, 8.16; N, 8.97; "molecular formula C$_{24}$H$_{37}$N$_3$O$_4$Si" requires C, 62.71; H, 8.11; N, 9.14%. $[\boldsymbol{\alpha}]_D^{20}$ = −11 (c, 1.0, CHCl$_3$). FT-IR (disk) $\nu$ = 3,313, 3,063, 3,030, 2,973, 2,925, 1,632, 1,590, 1,494, 1,453, 1,389, 1,256, 1,193, 1,165, 1,101, 1,075, 1,029, 955 cm$^{-1}$. $^1$H-NMR (400 MHz, CDCl$_3$, ppm) $\delta$: 0.33–0.37 (m, 2H), 1.03 (t, $J$ = 7.0 Hz, 9H), 1.30–1.37 (m, 2H), 1.81–1.88 (br, s, 2H), 2.88–2.93 (m, 2H), 3.61 (q, $J$ = 7.0 Hz, 6H), 4.46–4.48 (m, 1H), 5.59–5.60 (m, 1H), 7.03–7.06 (m, 2H), 7.05–7.09 (m, 5H), 7.11–7.14 (m, 7H). $^{13}$C-NMR (100 MHz, CDCl$_3$, ppm) $\delta$: 7.5 (CH$_2$), 18.2 (CH$_3$), 23.4 (CH$_2$), 42.9 (CH$_2$), 58.4 (CH$_2$), 60.2 (CH), 60.4 (CH), 126.6 (CH), 126.7 (CH), 127.3 (CH), 127.4 (CH), 128.4 (CH), 128.5 (CH), 141.2 (C), 142.3 (C), 157.9 (C). MS (MALDI-TOF) MS calculated [M + H]$^-$ for C$_{38}$H$_{41}$N$_3$O$_6$Si: 663.3 found: 663.7 [M + DIT(C$_{14}$H$_{10}$O$_3$)-4H]$^+$.

## 2.2.6 | Synthesis of mesoporous silica nanoparticles supported chiral urea-amine bifunctional catalysts (6–9)

Before the functionalization, the mesoporous silica nanoparticles were activated under vacuum at 120°C for 2 h. Compound **4** or **5** (0.08 g) in dry toluene (40 ml) was added dropwise to SBA-15 or mMCM-41 (1 g) under inert atmosphere at 25°C. The resulting mixture was stirred at 110°C for 20 h. Soxhlet extraction with dichloromethane for 20 h yielded mesoporous silica nanoparticles supported chiral urea-amine catalysts **6–9**. The supporting material of catalysts **6** and **7** was SBA-15, whereas mMCM-41 was for catalysts **8** and **9**.

## 2.2.7 | Screening of the catalytic activity of 4–9 in enantioselective transfer hydrogenation of aromatic ketones

To screen the catalytic activity of **3–9** in ATH of aromatic ketones, the general conditions applied for the reactions are as follows. [Ru(p-cymene)Cl$_2$]$_2$ was added to the solution of silyl derivatives **4** and **5** or organofunctionalized mesoporous silica nanoparticles **6–9** in 7 ml of isopropanol under inert atmosphere at 25°C. Then, the temperature was brought to 82°C, stirred for 2 h. After 2 h, the aromatic ketone was added to the reaction flask at 25°C, and then the temperature of reaction mixture was adjusted to 82°C. Base catalyzed ATH was initiated by adding of NaOH to the reaction mixture. To screen the conversions and enantiomeric excess, a few drops of reaction mixture were taken from the flask, diluted with isopropanol, and then filtered through microfilter. The filtrate was loaded on GC equipped with chiral column. The conversions and enantiomeric excess were calculated from the GC measurements by using the area under the peak corresponding to the ketone and its alcohol product.

## 2.2.8 | Screening of the catalytic activity of 4–9 in enantioselective Michael addition of acetylacetone to nitroolefins

To screen the catalytic activity of **4–9** in enantioselective Michael addition of acetylacetone to nitroolefins, the general conditions applied for the reactions are as follows. Silyl derivatives **4** and **5** or organofunctionalized mesoporous silica nanoparticles **6–9** were added to the solution of nitrostyrene derivative (0.2 mmol) in water/dry solvent and stirred for 10 min. Then, to this solution was added acetylacetone under inert atmosphere at 25°C and stirred for 48 h. After 48 h, catalysts **6–9** were recovered by either filtration or decantation. To screen the conversions and enantiomeric excess, samples were taken from the reaction content, diluted with isopropanol and then filtered through microfilter. The filtrate was loaded on high-performance liquid chromatography (HPLC) equipped with chiral column. The conversions and enantiomeric excess were calculated from the HPLC measurements by using the area under the peak corresponding to the nitroolefin derivatives and the product. The configuration of enantiomers was determined by comparing the retention times of our samples with the retention times reported in the literature.[59]

# 3 | RESULTS AND DISCUSSION

## 3.1 | Characterization of SBA-15, mMCM-41, and 6–9

The preparation of mesoporous silica nanoparticles supported chiral urea-amine bifunctional catalysts **6–9** were performed by following the steps described in Scheme 1. FT-IR spectroscopy was employed as the first step to characterize $Fe_3O_4$ magnetic nanoparticles, the mesoporous materials SBA-15, mMCM-41 and organofunctionalized mesoporous silica nanoparticles (**6–9**). Figure 1 presents the FT-IR spectra of $Fe_3O_4$, SBA-15, mMCM-41, and organofunctionalized mesoporous silica nanoparticles (**6–9**).

The overlaid FT-IR spectra of SBA-15 and solid catalysts **6** and **7** were given Figure 1a,b. The stretching, bending and out of plane signals of Si—O bonds were observed for SBA-15 at 1,082 (asymmetric stretching), 814 (symmetric stretching), and 458 cm$^{-1}$ (bending vibration), respectively. Silanol groups in the structure of these silica materials are characterized by the observed
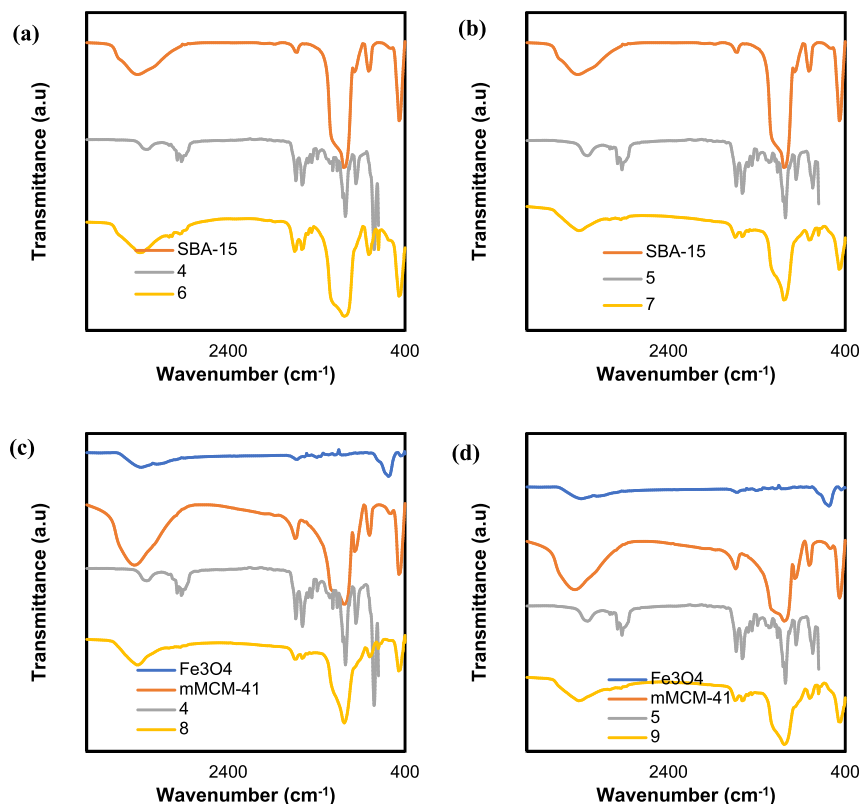
**SCHEME 1** Synthesis of mesoporous silica nanoparticles supported chiral urea-amine bifunctional catalysts **6–9**
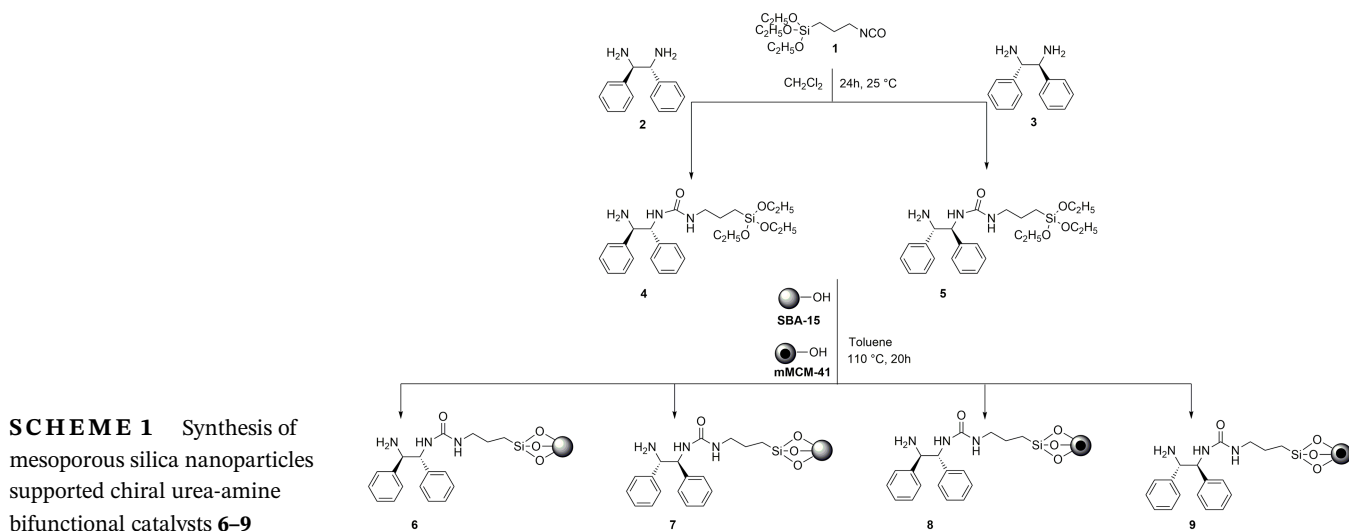
**FIGURE 1** FT-IR spectra of **3**, **6**, and **SBA-15** (a), FT-IR spectra of **5**, **7**, and **SBA-15** (b), FT-IR spectra of **3**, **8**, and **MCM-41** (c), FTIR spectra of **5**, **9**, and **MCM-41** (d)

vibrational band at 962 cm$^{-1}$. In addition to that, SBA-15 showed a band at 1,628 cm$^{-1}$ belonging to water adsorbed by SBA-15, and a band of 3,425 cm$^{-1}$ due to stretching from silanol groups in the structure of SBA-15. The compatibility of the values obtained in the FT-IR spectrum of the SBA-15 with the values in the literature confirms that the synthesis of SBA-15 have been successfully carried out.[60–62] The observation of new bands in FT-IR of **6** and **7** along with the preservation of IR bands responsible for SBA-15 support can be taken as a clear evidence for the incorporation of **4** and **5** to SBA-15. For example, the band at 3,064 cm$^{-1}$ was corresponded to the aromatic ring vibration of organic groups (**4** and **5**). The appearance of new band at around 2,930 and 2,867 cm$^{-1}$ was assigned to stretching vibration of —C—H from CH$_2$. Carbonyl group of urea structure for **6** and **7** gave clear vibrational band at 1,644 cm$^{-1}$, which also confirmed the successful functionalization of SBA-15. The stretching vibration of —NH and —NH$_2$ could not be observed because the stretching of O—H from Si—OH groups on the surface of mesoporous materials and from molecular water within pores overlapped in same region. All these FT-IR spectral data demonstrate that chiral silyl derivatives **4** and **5** have been grafted onto the SBA-15, which were also verified laterally by TGA analysis.

The FT-IR spectra of Fe$_3$O$_4$, Fe$_3$O$_4$/MCM-41 (mMCM-41), **8** and **9** were presented in Figure 1c,d. The FT-IR spectra of Fe$_3$O$_4$ showed a characteristic stretching vibration at 567 cm$^{-1}$ corresponded to the Fe—O bond stretching vibration of Fe$_3$O$_4$. After coating MCM-41 shell, Fe$_3$O$_4$/MCM-41 composites (mMCM-41) exhibited three characteristic peaks at 1,078, 802, and 455 cm$^{-1}$, corresponded to the anti-symmetric, symmetric Si—O stretching and deformation mode of SiO$_4$ tetrahedral in the MCM-41 silica. The bending vibration of Si—OH group in the MCM-41 silica were characterized by the band located at 960 cm$^{-1}$. However, this characteristic IR absorption band was disappeared after incorporation of **4** and **5** onto mMCM-41, because Si—OH groups in mMCM-41 silica were reacted with the silyl groups of **4** and **5** to produce the heterogeneous solid catalysts **8** and **9**. As for the solid catalysts **8** and **9**, the observation of IR absorption band at 570 cm$^{-1}$ confirmed the presence of Fe—O bond in their structure as well.[30–35,63] In addition to that, the new IR absorption band at 1,635 cm$^{-1}$ can be easily attributed to stretching vibration mode of C=O bond. Moreover, the weak IR bands at 2,935 and 2,870 cm$^{-1}$ were due to the asymmetric and symmetric stretching vibration of —C—H bonds. The band at 3,038 cm$^{-1}$ was corresponded to the aromatic ring vibration of organic groups. The stretching vibration of —NH and —NH$_2$ could not be observed due to the broad intense absorption of O—H groups from Si—OH groups on the surface of mesoporous materials and from molecular water within pores. Overall, these FT-IR results confirmed that covalent grafting of **4** and **5** onto mMCM-41 was performed successively.

Figure 2 shows the scanning electron microscope (SEM) images of mesoporous materials SBA-15, mMCM-41 and catalysts **6–9**. As can be seen from Figure 2a, SBA-15 has rod-like morphology aggregated into bundles as commonly observed in pure SBA-15 material.[64] After grafting of **4** and **5** onto SBA-15, no remarkable differences in the morphology was observed between bare SBA-15 and solid catalysts **6** and **7** (Figure 2c,e). The morphology of mMCM-41 and solid catalysts **8** and **9** were also studied by SEM technique. SEM images of these materials were shown in Figure 2b,d,f. Homogenous spherical morphology was observed for mMCM-41. As shown, the morphology of organofunctionalized mesoporous silica nanoparticles **8** and **9** were similar to the mMCM-41.

To determine the element contents of Fe$_3$O$_4$, SBA-15, mMCM-41 and **6–9**, energy dispersive X-ray analysis (EDX) and elemental scanning mappings measurements were performed. The EDX spectrum of SBA-15 showed that the structure of this mesoporous silica material contains only Si (24.9%) and O (75.1%), whereas mMCM-41 clearly exhibited the presence of Fe (0.2%) atom in its texture in addition to the Si (34.2%) and O (65.6%) atoms (see Supporting information for the images). Whereas only Fe and O were present in the texture of Fe$_3$O$_4$. Elemental scanning mapping measurement also confirms the presence of Si and O atoms for SBA-15, Fe and O atoms for Fe$_3$O$_4$, and Fe, Si and O atoms for mMCM41 in the structures of these materials (see Supporting information for the images). The solid catalysts **6** and **7** possessed the elements of Si, O, C, and N atoms in their texture, whereas mMCM-41 supported catalysts **8** and **9** had the element of Fe in addition to the elements of Si, O, C, and N atoms. As can be clearly observed from the EDX spectrum of **6–9**, after grafting of **4** and **5** onto the supporting material SBA-15 and mMCM-41, carbon and nitrogen contents were increased, whereas Fe and O contents were decreased (Figure 3a for **6** and Figure 3b for **8**). These results also confirmed the successful grafting of **4** and **5** onto the SBA-15 and mMCM-41. The elemental scanning mappings analyses were applied for the distribution of elements in **6–9**. The analyses clearly exhibited a homogenous distribution of elements content in the structure of **6–9** (Figure 4 for **8**, see Supporting information for the elemental scanning mappings of other catalysts).

The purity, phase and crystallinity of Fe$_3$O$_4$, SBA-15, mMCM-41, and **6–9** were measured by XRD technique. Low-angle XRD of SBA-15 and mMCM-41 are illustrated

**FIGURE 2** Scanning electron microscope (SEM) images of **SBA-15** (a), **mMCM-41** (b), **6** (c), **8** (d), **7** (e), and **9** (f)
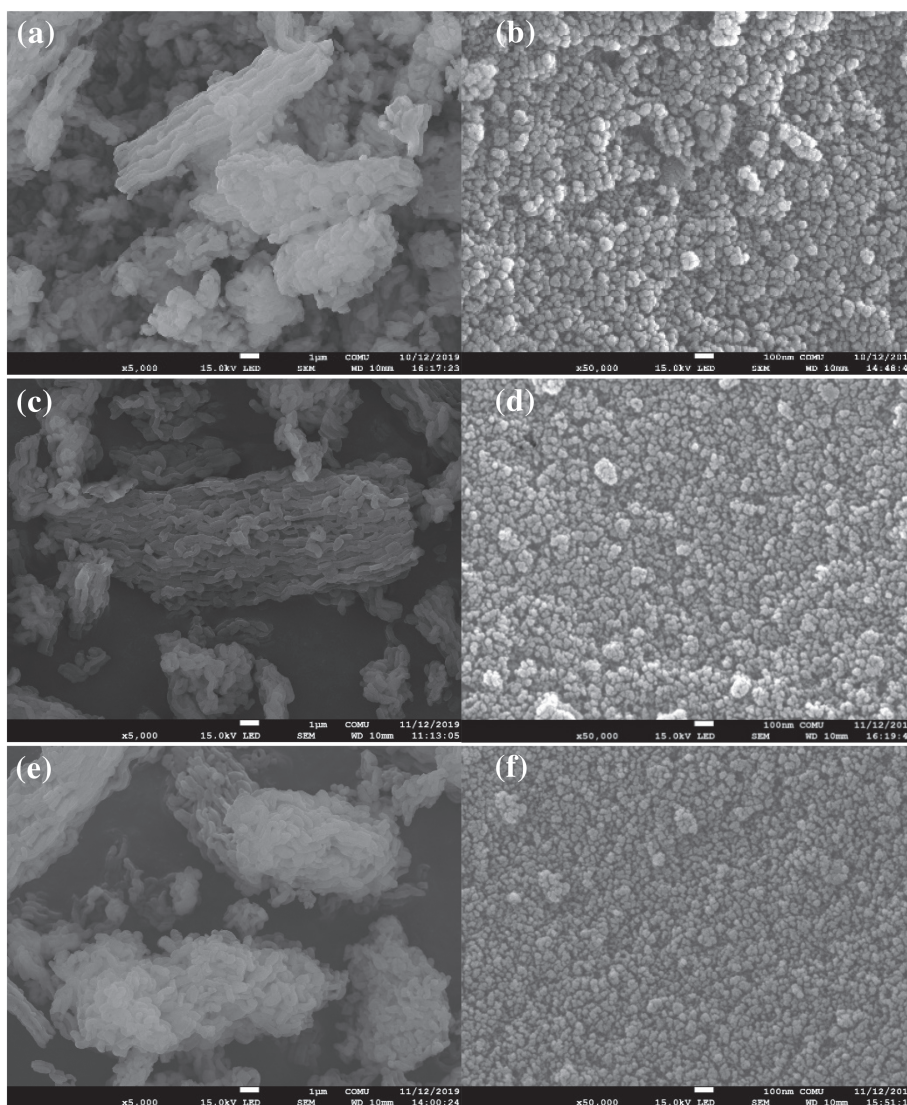


in Figure 5. Figure 5a shows the diffraction patterns recorded between $2\theta = 0.5$–$5°$ for parent material SBA-15 and solid catalysts **6–7**. All materials had same strong diffraction reflection (100) at $2\theta = 0.90°$, which were consistent with the characteristic peaks of a well-defined hexagonal symmetry of mesoporous silica SBA-15.[64,65] In addition to that intense peak, there were two low intensity peaks between $1.5°$ and $1.9°$. Noted that the position of (100) reflection line for SBA-15 was shifted to a large angle compared with the solid catalysts **6** and **7**. Also noted that the intensities of (100) peak of **6** and **7** were lower than SBA-15 supporting material, but the shape of the signal of **6** and **7** was the same as the shape of the signal of SBA-15. All these results confirmed that the synthesis of heterogeneous chiral catalysts **6** and 7 was obtained successfully by the incorporation of organic material onto SBA-15. The XRD patterns of $Fe_3O_4$, mMCM-41, **8** and **9** were shown in Figure 5b–d. According to the wide angle XRD pattern of $Fe_3O_4$ in

Figure 5c, $Fe_3O_4$ nanoparticles presented peaks at $30.5°$, $36.1°$, $42.4°$, $57.3°$, and $63.2°$, attributing the typical reflections of (220), (311), (422), (511), and (440) crystallographic planes of $Fe_3O_4$, respectively, which corresponded to the values of the main peaks of $Fe_3O_4$ nanoparticles presented in the JCPDS database file, No.85-1436.[29–34] After the surface modification of $Fe_3O_4$ nanoparticles with MCM-41, the same characteristic peaks of $Fe_3O_4$ appeared in the wide angle XRD of mMCM-41, but the intensity of the main peaks of $Fe_3O_4$ decreased because the molar ratio of $Fe_3O_4$ was relatively low in the structure of mMCM-41 compared with the pure $Fe_3O_4$. The broad peak at $20°$–$30°$ can be attributed to the silica skeleton in mMCM-41 (Figure 5c). After immobilization of chiral compounds **4** and **5** onto mMCM-41, the same characteristic of the peaks of $Fe_3O_4$ and MCM-41 was observed in the wide angle XRD pattern of **8** and **9**. These results confirmed that the modification of mMCM-41 did not change the crystal phase of
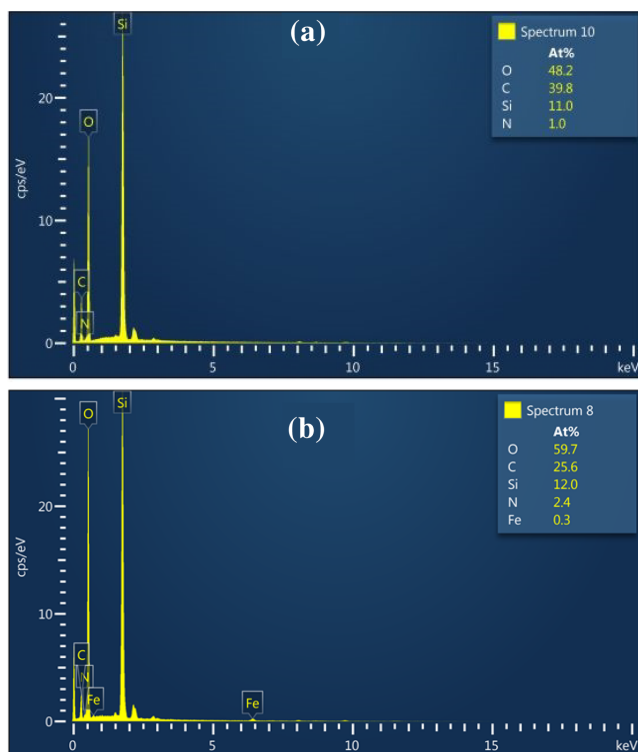
**FIGURE 3** Energy dispersive X-ray analysis (EDX) diagrams of (a) **6** and (b) **8**

$Fe_3O_4$ particles (Figure 5d). To understand the mesoporous nature of the mMCM-41 and catalysts **8** and **9**, the low angle XRD analyses of mMCM-41 catalysts **8** and **9** were performed and the results were presented in Figure 3b. All three materials showed strong diffraction reflection (100) at $2\theta = 2.4°$. The presence of strong diffraction reflection in their XRD patterns can be attributed to the regularity of mesoporous channels of MCM-41.[29–34] Grafting of organic groups (**4** and **5**) onto mMCM-41 resulted in lower intensity of characteristic peaks for **8** and **9** compared with the peak of mMCM-41. But, observation of the same characteristic peak for **8** and **9** confirms no loss of structural ordering. The successful immobilization of organic layers onto supporting material mMCM-41 was also confirmed by these obtained results.

The structural parameters of SBA-15, mMCM-41, and **6–9** were calculated from $N_2$ adsorption–desorption measurements and given in Table 1. Adsorption–desorption isotherms with the distribution curves of pore size for SBA-15, mMCM-41 and **6–9** were given in Figure 6. According to IUPAC adsorption isotherm classification, $N_2$ sorption isotherms of SBA-15, mMCM-41 and **6–9** were in agreement with a type IV adsorption isotherm with an H1 hysteresis.[66] The amount of $N_2$ adsorption showed an increase at $0.6 < P/P_0 < 0.7$ for

SBA-15, **6**, and **7**, and $0.2 < P/P_0 < 0.3$ for mMCM-41, **8**, and **9**. Bare mesoporous materials have bigger surface area and larger pore volume than those for organofunctionalized **6–9**. As seen from Table 1, SBA-15 had a surface area of 459 $m^2$ $g^{-1}$, pore volume of 0.51 $cm^3$ $g^{-1}$ and the average pore size of 5.68 nm, whereas mMCM-41 supports possessed a surface area of 1,129 $m^2$ $g^{-1}$, pore volume of 0.61 $cm^3$ $g^{-1}$ and the average pore size of 2.57 nm. As expected, prepared catalysts **6–9** had smaller surface area and pore volume compared with the parent supports, which proved that organic groups (**4** and **5**) were successfully incorporated into SBA-15 and mMCM-41 (Table 1).

TGA of SBA-15, mMCM-41, and **6–9** were performed to calculate the amount of grafted organic groups (**4** and **5**) onto SBA-15 and mMCM-41. The obtained TGA curves of SBA-15, mMCM-41, and **6–9** are shown in Figure 7. The calculated amounts of organic groups of **6–9** are presented in Table 2. TGA curves of bare SBA-15 and mMCM-41 have two distinct regions of weight loss. The first region was observed between 20°C and 150°C. Mass lost in this region can be attributed to the removal of water and organic solvents both on the surface and within the pores of silica. The second mass loss region was observed between 150°C and 650°C. The weight loss was calculated as ~2%. TGA curves in this region are nearly flat. The 2% of weight loss was attributed to the silanol condensation.[22,29–34] In the TGA analysis of **6–9**, the first weight loss was observed below 200°C because of the solvents and water on the surface and within the pores of **6–9**.[67–69] It is very obvious from TGA curves that the weight loss of **6–9** in the first region show a decreased value compared with the first region of bare mesoporous materials with **6–9**, indicating that **6–9** have higher hydrophobic character than bare mesoporous materials.[70] After that, the weight loss in the second region between 150°C and 600°C can be attributed to the decomposition of covalently bounded organic groups (**4** and **5**) within the pores. The amount of grafted organic groups (**4** and **5**) onto SBA-15 and mMCM-41 was estimated to be 0.16 mmol $g^{-1}$ from the TGA curves.

## 3.2 | Catalytic studies

### 3.2.1 | Catalytic activity for enantioselective transfer hydrogenation

The catalytic activities of the Ru(II) complexes of the obtained chiral organic groups (**4** and **5**) and **6–9** were tested in enantioselective transfer hydrogenation (ATH) of various aromatic ketones. During the performing of these reactions, the Ru(II) complexes of chiral organic
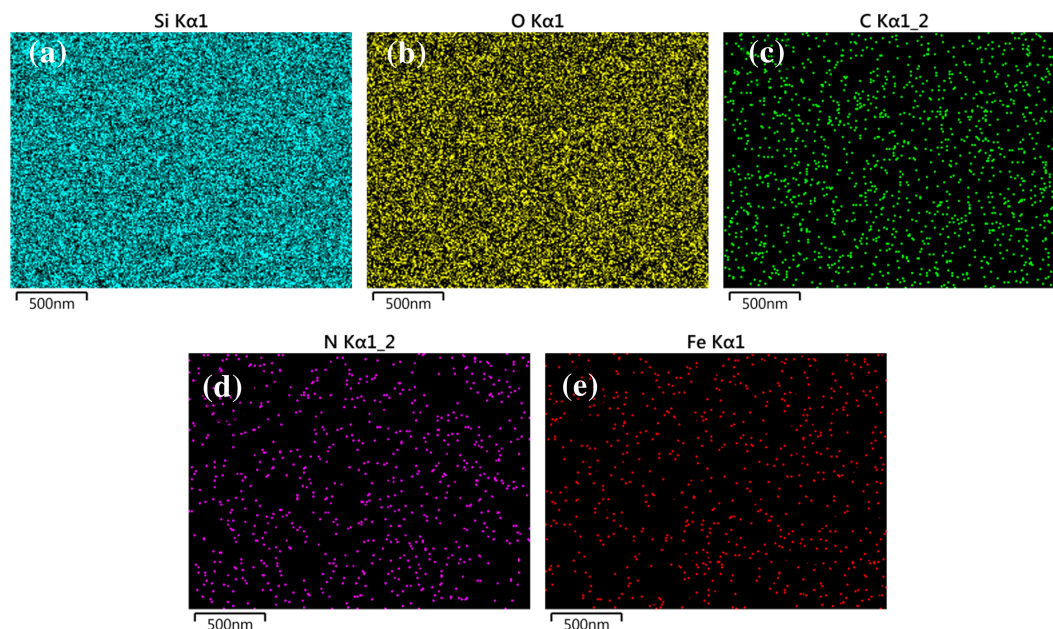
**FIGURE 4** Elemental scanning mappings of (a) silica, (b) oxygen, (c) carbon, (d) nitrogen, and (e) iron of **8**

**FIGURE 5** Low-angle X-ray diffraction (XRD) patterns of SBA-15, **6**, and **7** (a), mMCM-41, **8**, and **9** (b) and, wide-angle XRD patterns of mMCM-41 and $Fe_3O_4$ (c), mMCM-41, **8**, and **9** (d)
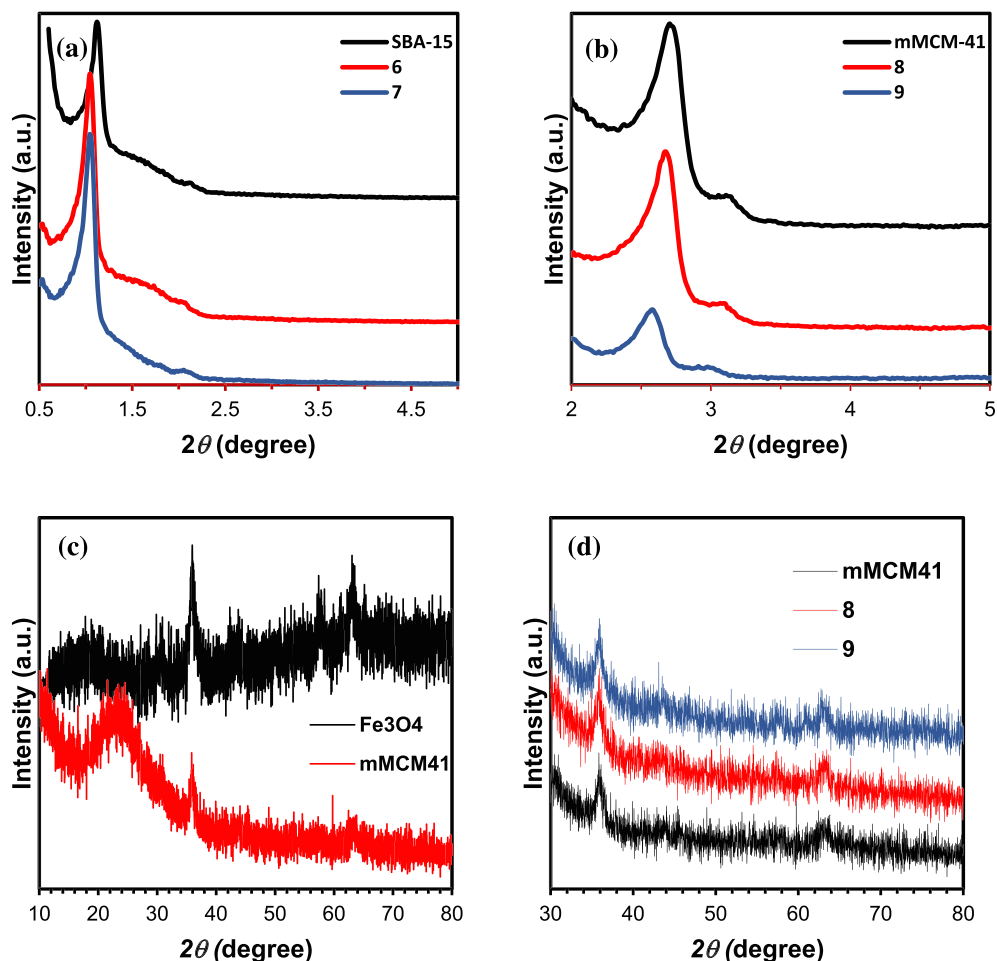


groups (**4** and **5**) and **6–9** were prepared in situ. For this, chiral organic groups (**4** and **5**) or **6–9** and [RuCl₂(*p*-cymene)]₂ were mixed in isopropyl alcohol (^*i*PrOH) for 2 h at 82°C. Enantioselective transfer hydrogenation reactions were carried out by adding ketone and base on those complexes prepared in situ.

**TABLE 1** Structural parameters of SBA-15, mMCM-41, and **6–9**

| Samples | $S_{BET}$ (m$^2$ g$^{-1}$)[a] | $D_p$ (nm)[b] | $V_p$ (cm$^3$ g$^{-1}$)[c] |
|---|---|---|---|
| SBA-15 | 459 | 5.68 | 0.51 |
| **(6)** | 327 | 5.59 | 0.39 |
| **(7)** | 338 | 5.61 | 0.40 |
| mMCM-41 | 1,129 | 2.57 | 0.61 |
| **(8)** | 995 | 2.43 | 0.51 |
| **(9)** | 930 | 2.43 | 0.50 |

[a]$S_{BET}$ = surface area, calculated BET method.
[b]$D_p$ = pore diameter, calculated BJH method.
[c]$V_p$ = pore volume.

To determine the optimum reaction conditions for the best catalytic activity, the ATH reaction of acetophenone was chosen as the model in the presence of **4**. To find the substrate/catalyst/base (s/c/b) ratios where catalysts can work most effectively, a series of test reactions were performed. The ratios of s/c/b used in the test reactions and the conversion values obtained are shown in Table 3.

The initial condition for the first entry was determined as follows: $^i$PrOH as hydrogen donor, NEt$_3$ as the base and substrate/catalyst (S/C) ratio as 250/1. When the s/c ratio is 250/1, the amount of 0.05, 0.1, 0.2, 0.4, 0.8, and 1 mmol of the NEt$_3$ base was added to the reaction medium, the effectiveness of the ruthenium complex of chiral urea-amine bifunctional catalyst **4** in the ATH reaction of acetophenone was determined by GC analysis (Table 3, entries 1–6). The highest conversion of acetophenone to the corresponding alcohol was obtained in the reaction conditions where the amount of NEt$_3$ in the reaction was 0.4 mmol. A decrease in the conversion values of acetophenone was observed when NEt$_3$ was used less or more than 0.4 mmol. When the enantioselectivity results of these reactions were examined, it was observed that the product was obtained in all reactions. Without NEt$_3$ or catalyst **4** under identical conditions, 1-phenylethanol was obtained with the conversions of 47% and 60%, respectively. Moreover, no reaction occurred between acetophenone and isopropyl alcohol in the absence of [RuCl$_2$(p-cymene)]$_2$ (Table 3, entry).

After finding the ratio of base as 0.4 mmol, the effect of base type on the catalytic activity of **4** was studied by using NaOH, KOH, and $^t$BuOK under the same reaction conditions. As seen from Table 3, all three bases have lower conversion rates than NEt$_3$ after 24-h reaction times. However, NaOH, KOH, and $^t$BuOK bases were able to catalyze the reaction enantioselectively, unlike NEt$_3$. The highest conversion (89%) and enantioselectivity (56% *ee*) were obtained in the presence of NaOH as base (Table 3, entry 12). Our final effort involves determining the best catalyst/substrate ratio for this model reaction. A decrease or an increase in the amount of catalyst compared with 250/1 afforded the product with lower conversion and enantioselectivity as seen from entries 13–15 in Table 3.

To investigate the scope of chiral ligands **4** and **5**, and **6–9** in ATH, the reduction of a series of aromatic ketones to their corresponding alcohols was studied under the optimized conditions (82°C, s/c = 250/1, NaOH as the base) (Table 3, entry 12). In the case of **4** and **5**, the highest catalytic activities were obtained in the ATH reaction of 4′-chloroacetophenone and 4′-bromoacetophenone with poor enantioselectivities (Table 4, entries 19, 25 for **4** and 20, 26 for **5**). Changing the substituent at *p*-position of the aromatic ketone from chlorine or bromine to methyl or methoxy, the reactions catalyzed **4** and **5** afforded chiral alcohols in moderate conversion but with better enantioselectivities (Table 4, entries 7, 13 for **4** and 8, 14 for **5**). The highest enantioselectivity was obtained as 65% *ee* within 2 h in reaction of 4′-methylacetophenone catalyzed with **4** (Table 4, entry 13).

To able to compare the catalytic activity of **6–9** with their homogenous counterparts **4** and **5**, **6–9** were tested in the same reactions after coordination with [Ru(p-cymene)Cl$_2$]$_2$. The catalytic results of **6–9** were also summarized in Table 4. The obtaining acceptable enantioselectivity under the similar reaction conditions demonstrate the chiral recognition ability of **6–9**. Among the results, the highest enantioselectivity was obtained as 57% *ee* in the reaction of acetophenone within 2 h in the presence of **8**, which is a comparable result with the result of its homogeneous counterpart **4** (Table 4, entry 5).

But the enantioselectivity was decreased to 37% *ee* by further increasing the reaction time to 24 h (Table 4, entry 5). The same reaction was catalyzed by **9** with 30% *ee* (Table 4, entry 6). The morphology of **9** was very similar with that of **8** according to the XRD, SEM, and BET measurements. Showing very close catalytic activity of **8** and **9** in ATH of aromatic ketones can be attributed to their structural similarities. Under similar reaction conditions, catalysts **6** and **7** gave lower conversions and enantioselectivities compared with the results of **8** and **9** (Table 4, entries 3 and 4). Heterogeneous catalysts **6** and **7** were obtained by grafting of **4** and **5** onto SBA-15. As seen in Table 1, the catalysts **8** and **9** have a much higher BET surface area and pore volume than catalysts **6** and **7**. The poor catalytic activities of **6** and **7** can be due to their low BET surface area and pore volume which cause slower reaction rates and slow diffusion of guest

**FIGURE 6** N$_2$ adsorption–desorption isotherms of SBA-15, **6**, and **7** (a), mMCM-41, **8**, and **9** (b) and, pore size distribution for SBA-15, **6**, and **7** (c) mMCM-41, **8**, and **9** (d)
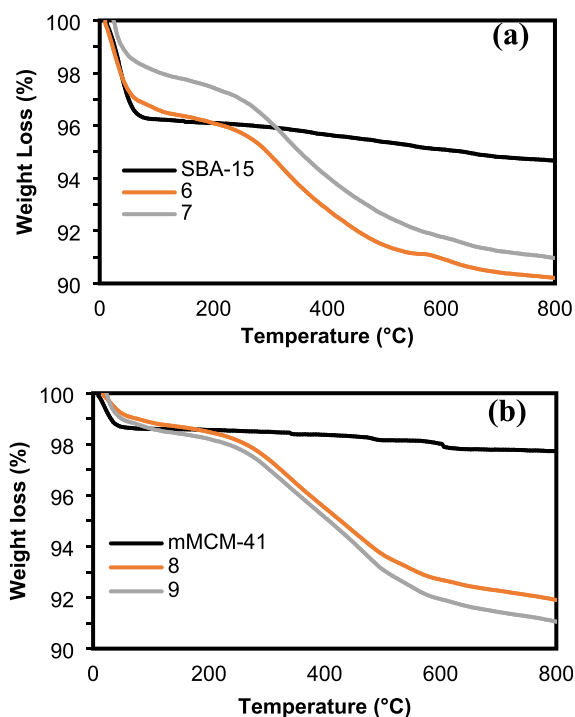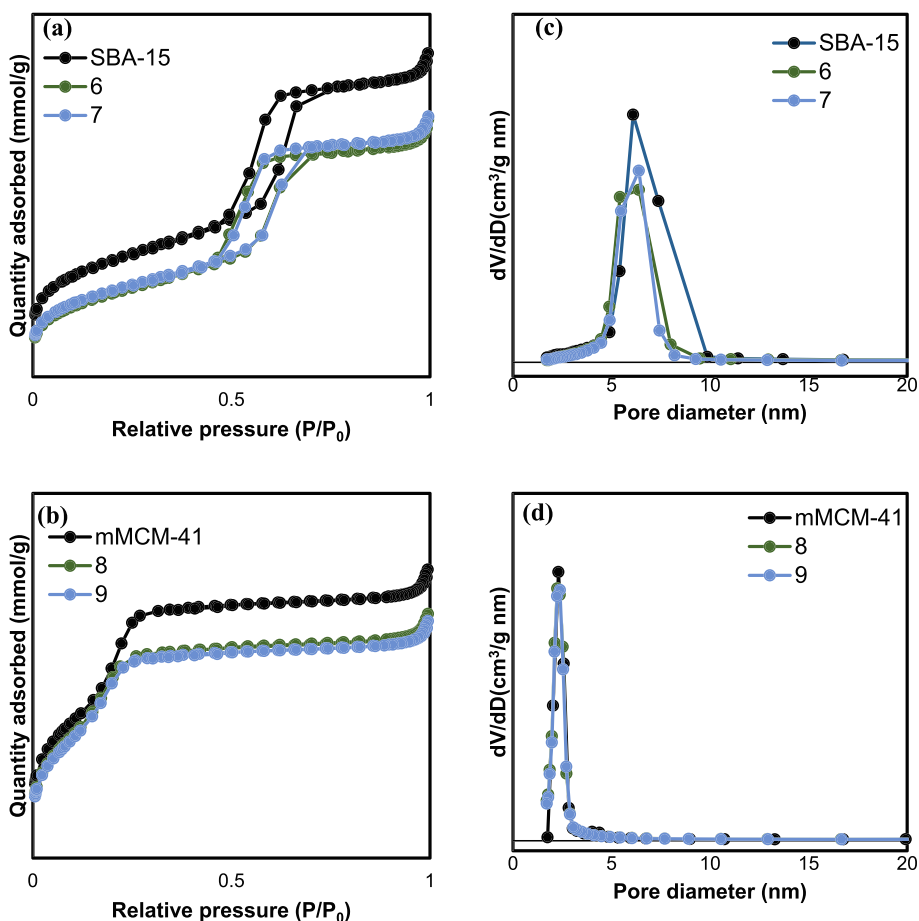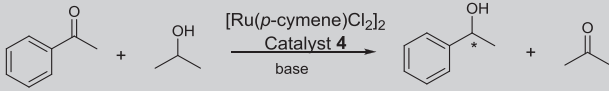
**FIGURE 7** Thermogravimetric analysis (TGA) analysis of SBA-15, **6**, and **7** (a); MCM-41, **8**, and **9** (b)

**TABLE 2** Percentage of weight loss of SBA-15, mMCM-41, and **6–9** versus temperature

| Samples | Weight loss (% w/w) | | Residuals > 650°C (% w/w) |
| | 20°C–150°C | 150°C–750°C | |
| --- | --- | --- | --- |
| SBA-15 | 3.8 | 1.4 | 94.8 |
| (**6**) | 3.6 | 7.1 | 85.7 |
| (**7**) | 2.2 | 6.9 | 88.7 |
| mMCM-41 | 6.7 | 1.1 | 92.2 |
| (**8**) | 1.3 | 7.1 | 91.6 |
| (**9**) | 1.6 | 7.2 | 91.2 |

molecules throughout the mesoporous matrix during the catalytic process.[71–73] The experimental results showed that the structural morphology of mesoporous silica nanoparticles has important effect on the performance of heterogeneous catalysts.

The rate and enantioselectivity in enantioselective transfer hydrogenation reaction are sensitive to the steric and electronic properties of the substrate because the transfer hydrogenation is reversible.[74,75] The results

**TABLE 3** Reaction optimization for enantioselective transfer hydrogenation of acetophenone



| Entry | Time (h) | Base | mmol | Conversion (%)[a] | % ee[b] | TON[c] |
|---|---|---|---|---|---|---|
| 1 | 2 (24) | $NEt_3$ | 0.05 | 66 (89) | ras | 223 |
| 2 | 2 (24) | $NEt_3$ | 0.1 | 52 (70) | ras | 175 |
| 3 | 2 (24) | $NEt_3$ | 0.2 | 45 (55) | ras | 138 |
| 4 | 2 (24) | $NEt_3$ | 0.4 | 86 (98) | ras | 245 |
| 5 | 2 (24) | $NEt_3$ | 0.8 | 31 (56) | ras | 140 |
| 6 | 2 (24) | $NEt_3$ | 1 | 32 (44) | ras | 110 |
| 7[d] | 2 (24) | - | - | 7 (47) | ras | 118 |
| 8[e] | 24 | $NEt_3$ | 0.4 | - | - | - |
| 9[f] | 24 | $NEt_3$ | 0.4 | 60 | ras | 150 |
| 10 | 2 (24) | KOH | 0.4 | 10 (41) | 53 (15)(R) | 103 |
| 11 | 2 (24) | t-BuOK | 0.4 | 16 (54) | 55 (20)(R) | 135 |
| 12 | 2 (24) | NaOH | 0.4 | 46 (89) | 56 (33)(R) | 223 |
| 13[g] | 2 (24) | NaOH | 0.4 | 27 (80) | 49/18(R) | 200 |
| 14[h] | 2 (24) | NaOH | 0.4 | 11 (75) | 3/ras | 188 |
| 15[i] | 2 (24) | NaOH | 0.4 | 11 (67) | ras | 168 |

*Note.* Reactions were performed by using 1 mmol acetophenone in 7 ml of *i*PrOH with Ru:ligand = 1:2. Substrate/catalyst ratio was 250/1 for the entries 1–12.

[a]Determined by GC (HP-Chiral-20B).

[b]Absolute configuration was confirmed by comparing the retention times of the enantiomers on the GC traces with that reported in the literature.

[c]TON (Turnover number) = [moles of desired product (chiral secondary alcohol) formed]/[moles of catalyst used].

[d]In the absence of $NEt_3$.

[e]In the absence of $[RuCl_2(p\text{-cymene})]_2$.

[f]In the absence of catalyst **4**.

[g]Substrate/catalyst ratio was 125/1.
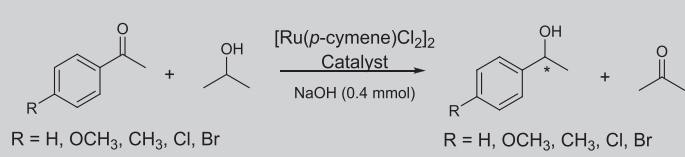
[h]Substrate/catalyst ratio was 500/1.

[i]Substrate/catalyst ratio was 1,000/1.

from Table 4 were aroused that the introduction of electron withdrawing substituents such as chlorine or bromine atom to the *p*-positions of related aromatic ketones resulted in higher conversion (99%) and poor enantioselectivity (*ras*-18% *ee*), whereas the presence of an electro-donating group such as methyl or methoxy at the *p*-position of aromatic ketones tended to lower catalytic activity (31%–70%) and moderate enantioselectivity (65% *ee*) (Table 4, entries 7–30). It has been also observed that sterically larger groups lead to a decrease in reaction rate and enantioselectivity, regardless of their electron withdrawing or electro-donating properties.

Additionally, the conversion of aromatic ketones increased sharply with the prolonged reaction time, but the higher conversion resulted in lower enantioselectivities. It was mentioned above that the transfer hydrogenation of

ketones was reversible.[74,75] Noted that all *ee* values obtained within 2 h were higher than the values obtained within 24 h, which are in agreement with the literature explanations. On the other hand, considering the 24-h period, **6–9** exhibited comparable enantioselectivity but lower catalytic activity than their homogeneous counterparts **4** and **5**. The poor catalytic activity of **6–9** can be explained by irregularly distributed **4** and **5** onto the MSNs, which makes the access of substrate to the active site difficult.[71–73]

The influence of increased amount of **6–9** on conversion and enantioselectivity was investigated in the ATH of acetophenone and summarized in Table 5. A sharp increase of catalytic activity in all cases was observed upon increasing S/C ratio. The catalytic activity in the case of **8** and **9** reached to 87% and 85% within 24 h

**TABLE 4** Ru-catalyzed enantioselective transfer hydrogenation of ketones with chiral urea-amine bifunctional ligand **4**, **5**, and their heterogeneous counterparts **6–9**
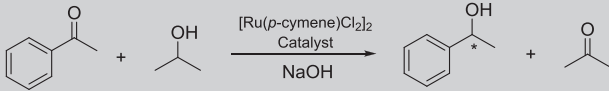


R = H, OCH₃, CH₃, Cl, Br

| Entry | R | Cat | Time (h) | Conversion (%)[a] | % ee[b] | TON[c] |
|---|---|---|---|---|---|---|
| **1** | H | **4** | 2 (24) | 46 (89) | 56 (33)(R) | 223 |
| **2** | H | **5** | 2 (24) | 14 (70) | 22 (4)(S) | 175 |
| **3** | H | **6** | 2 (24) | 23 (27) | 12 (10)(R) | 68 |
| **4** | H | **7** | 2 (24) | 14 (22) | 27 (10)(S) | 55 |
| **5** | H | **8** | 2 (24) | 12 (18) | 57 (37)(R) | 45 |
| **6** | H | **9** | 2 (24) | 26 (30) | 37 (30)(S) | 75 |
| **7** | OCH₃ | **4** | 2 (24) | 26 (46) | 57 (25)(R) | 115 |
| **8** | OCH₃ | **5** | 2 (24) | 8 (31) | 49 (20)(S) | 78 |
| **9** | OCH₃ | **6** | 2 (24) | 11 (12) | 2 (1)(R) | 30 |
| **10** | OCH₃ | **7** | 2 (24) | 6 (8) | 27 (18)(S) | 20 |
| **11** | OCH₃ | **8** | 2 (24) | 6 (11) | 36 (5)(R) | 28 |
| **12** | OCH₃ | **9** | 2 (24) | 21 (27) | 38 (35)(S) | 68 |
| **13** | CH₃ | **4** | 2 (24) | 42 (70) | 65 (38)(R) | 175 |
| **14** | CH₃ | **5** | 2 (24) | 14 (57) | 47 (10)(S) | 143 |
| **15** | CH₃ | **6** | 2 (24) | 17 (19) | 14 (9)(R) | 48 |
| **16** | CH₃ | **7** | 2 (24) | 16 (31) | 33 (16)(S) | 78 |
| **17** | CH₃ | **8** | 2 (24) | 13 (22) | 54 (31)(R) | 55 |
| **18** | CH₃ | **9** | 2 (24) | 30 (38) | 41 (32)(S) | 95 |
| **19** | Cl | **4** | 2 (24) | 62 (99) | 32 (18)(R) | 248 |
| **20** | Cl | **5** | 2 (24) | 43 (98) | 31 (16)(S) | 245 |
| **21** | Cl | **6** | 2 (24) | 16 (35) | 31 (6)(R) | 88 |
| **22** | Cl | **7** | 2 (24) | 16 (34) | 32 (11)(S) | 85 |
| **23** | Cl | **8** | 2 (24) | 30 (56) | 47 (20)(R) | 140 |
| **24** | Cl | **9** | 2 (24) | 27 (43) | 59 (34)(S) | 108 |
| **25** | Br | **4** | 2 (24) | 38 (99) | *ras* | 248 |
| **26** | Br | **5** | 2 (24) | 40 (94) | 38 (18)(S) | 235 |
| **27** | Br | **6** | 2 (24) | 17 (44) | 31 (4)(R) | 110 |
| **28** | Br | **7** | 2 (24) | 7 (21) | 30 (5)(S) | 53 |
| **29** | Br | **8** | 2 (24) | 17 (40) | 42 (15)(R) | 100 |
| **30** | Br | **9** | 2 (24) | 23 (43) | 47 (17)(S) | 108 |

*Note*. Reactions were performed by using 1 mmol acetophenone in 7 ml of $^i$PrOH with Ru:ligand = 1:2; Substrate/catalyst ratio was 250/1 for all entries.

[a]Determined by GC (HP-Chiral-20B).

[b]Absolute configuration was confirmed by comparing the retention times of the enantiomers on the GC traces with that reported in the literature.

[c]TON (Turnover number) = [moles of desired product (chiral secondary alcohol) formed]/[moles of catalyst used].

**TABLE 5** The effect of catalyst amount on Ru-catalyzed ATH of acetophenone with **6–9** and recyclability of **6–9**



| Entry | S/C | Run | Catalyst | Conversion (%)[a, b] | % ee[c] | TON[d] |
|---|---|---|---|---|---|---|
| 1 | 125/1 | 1 | 6 | 30 (38) | 58 (50)(R) | 48 |
| 2 | 125/1 | 2 | 6 | 1 (3) | ras | 4 |
| 3 | 83/1 | 1 | 6 | 40 (60) | 57 (46)(R) | 50 |
| 4 | 62/1 | 1 | 6 | 54 (75) | 52 (44)(R) | 47 |
| 5 | 125/1 | 1 | 7 | 17 (33) | 43 (31)(S) | 41 |
| 6 | 125/1 | 2 | 7 | 1 (2) | ras | 3 |
| 7 | 83/1 | 1 | 7 | 20 (49) | 40 (23)(S) | 41 |
| 8 | 62/1 | 1 | 7 | 24 (71) | 40 (20)(S) | 44 |
| 9 | 125/1 | 1 | 8 | 27 (80) | 36 (21)(R) | 100 |
| 10 | 125/1 | 2 | 8 | 3 (5) | 12 (2)(R) | 6 |
| 11[e] | 125/1 | 3 | 8 | (85) | ras | 106 |
| 12[f] | 83/1 | 1 | 8 | 34 (87) {95} | 37 (24){22}(R) | 80 |
| 13 | 125/1 | 1 | 9 | 13 (31) | 42 (16)(S) | 26 |
| 14 | 125/1 | 2 | 9 | 2 (6) | 8 (5)(S) | 8 |
| 15 | 83/1 | 1 | 9 | 24 (61) | 36 (22)(S) | 51 |
| 16 | 62/1 | 1 | 9 | 38 (85) | 34 (24)(S) | 53 |

*Note.* Reactions were performed by using 1 mmol acetophenone in 7 ml of *i*PrOH with Ru:catalyst = 1:2.

[a]Determined by GC (HP-Chiral-20B).

[b]Results at second hour of the reactions are shown outside of brackets and those of 24th hour are in brackets.

[c]TON (Turnover number) = [moles of desired product (chiral secondary alcohol) formed]/[moles of catalyst used].

[d]Absolute configuration was confirmed by comparing the retention times of the enantiomers on the GC traces with that reported in the literature.

[e]0.004 mmol of [Ru(*p*-cymene)Cl$_2$]$_2$ was added at the third run of **8**.

[f]The reaction was followed for 48 h and the conversion at 48th hour was given in {}.

(Table 5, entries 12 and 16). In this case, an increase in the amount of **8** and **9** for ATH of acetophenone has a slight influence on enantioselectivity (Table 5, entries 9, 11, 12 for **8** and 13, 15, 16 for **9**). On the other hand, SBA-15 supported catalysts **6** and **7** showed a significant improvement in enantioselectivity when S/C was increased (Table 5, entries 1, 3, 4 for **6** and 5, 7, 9 for **7**).

The increasing S/C ratio of **6** from 250/1 to 62/1 resulted in 75% conversion with the highest enantioselectivity (44% *ee*) for a 24 h reaction period. The similar trend was also observed in the case of **7** (Table 5, entry 8). SBA-15 supported catalysts **6** and **7** showed a remarkable improvement in enantioselectivity when compared with the mMCM-41 supported catalysts **8** and **9**. SBA-15 supported catalysts **6** and **7** have a pore volume of ~0.40 cm$^3$ g$^{-1}$, whereas the mMCM-41 supported catalysts **8** and **9** have ~0,51 cm$^3$ g$^{-1}$, but pore diameters of

**6** and **7** were higher than **8** and **9** which makes the access of the substrate to the catalyst surface easy. The low catalytic activity of **6** and **7** comparing to the **8** and **9** was due to their low BET surface areas and pore volumes which have big influences on the reaction rates and needed longer reaction time as mentioned before according to the published literature.[71–73]
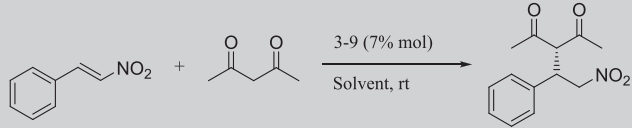
The reusability of **6–9** was investigated in the reaction of acetophenone and *i*PrOH. After the reactions, the SBA-15 supported catalysts **6** and **7** were separated from the reaction mixture by simple filtration, whereas the mMCM-41 supported catalysts **8** and **9** were separated by decantation because they contained magnetic Fe$_3$O$_4$ in their mesoporous structure. The recovered **6–9** were then subjected to the washing with water and drying under vacuum and then used in the next run without any treatment. The dramatical decrease in the

catalytic activity and enantioselectivity might be the result of leaching of Ru metal from **6–9**. To check the leaching of ruthenium from the support, [Ru(p-cymene)Cl$_2$]$_2$ was further added to the third run of **8** (Table 5, entry 12). No observation of enantioselectivity showed that catalyst **8** lost its activity irreversibly during the recycling route.[76]

## 3.2.2 | Catalytic activity for enantioselective Michael reaction

The catalytic activity of four supported catalysts **6–9**, and their homogeneous counterparts **4** and **5** was investigated in enantioselective Michael reaction. Initially, the blank experiments were performed in different

**TABLE 6** Screening of the reaction conditions for enantioselective Michael addition of acetylacetone to trans-β-nitrostyrene

| Entry | Catalyst | Solvent | Conversion (%)[a] | ee (%)[b] | TON[c] |
|---|---|---|---|---|---|
| 1 | SBA-15 | H$_2$O | - | - | - |
| 2 | SBA-15 | CH$_2$Cl$_2$ | - | - | - |
| 3 | SBA-15 | Toluene | - | - | - |
| 4 | mMCM-41 | H$_2$O | - | - | - |
| 5 | mMCM-41 | CH$_2$Cl$_2$ | - | - | - |
| 6 | mMCM-41 | Toluene | - | - | - |
| 7 | 4 | H$_2$O | 91 | 5 | 13 |
| 8 | 4 | CH$_2$Cl$_2$ | 15 | 10 | 2 |
| 9 | 4 | Toluene | 28 | 15 | 4 |
| 10 | 5 | H$_2$O | 96 | 3 | ∼14 |
| 11 | 5 | CH$_2$Cl$_2$ | 8 | 26 | 1 |
| 12 | 5 | Toluene | 7 | 11 | 1 |
| 13 | 6 | H$_2$O | 94 | 7 | 13 |
| 14[d] | 6 | H$_2$O | 87 | 5 | 12 |
| 15[e] | 6 | H$_2$O | 98 | 9 | ∼14 |
| 16 | 6 | CH$_2$Cl$_2$ | 15 | rac | 4 |
| 17 | 6 | Toluene | 30 | rac | 8 |
| 18 | 7 | H$_2$O | 92 | 5 | 13 |
| 19 | 7 | CH$_2$Cl$_2$ | 16 | 5 | 4 |
| 20 | 7 | Toluene | 43 | rac | 6 |
| 21 | 8 | H$_2$O | 92 | 5 | 13 |
| 22 | 8 | CH$_2$Cl$_2$ | 15 | 10 | 4 |
| 23 | 8 | Toluene | 28 | 15 | 4 |
| 24 | 9 | H$_2$O | 97 | 3 | ∼14 |
| 25 | 9 | CH$_2$Cl$_2$ | 22 | rac | 3 |
| 26 | 9 | Toluene | 51 | 2 | 7 |

*Note.* Reactions were performed by using trans-β-nitrostyrene (0.2 mmol) and acetylacetone (0.4 mmol).
[a]Isolated yield.
[b]Enantiomeric excess was determined by HPLC analysis using YMC chiral ART Amylose-C column.[22]
[c]TON (Turnover number) = [moles of desired product (chiral secondary alcohol) formed]/[moles of catalyst used].
[d]Reactions were performed at 50°C.
[e]The amount of catalyst was doubled.

**TABLE 7** Enantioselective Michael addition of acetylacetone to representative trans-β-nitrostyrene derivatives



R= 2-Br (**10**), 4-Br (**11**), 2-MeO (**12**), 4-MeO (**13**)

| Entry | R | Catalyst | Conversion (%)[a] | ee (%)[b] | TON[c] |
|---|---|---|---|---|---|
| 1 | 2-Br(**10**) | **6** | 55 | 6 | ∼8 |
| 2 | 2-Br(**10**) | **7** | 72 | rac | 10 |
| 3 | 2-Br(**10**) | **8** | 56 | 4 | 8 |
| 4 | 2-Br(**10**) | **9** | 88 | 3 | 13 |
| 5 | 4-Br(**11**) | **6** | 40 | 8 | ∼6 |
| 6 | 4-Br(**11**) | **7** | 50 | 10 | 7 |
| 7 | 4-Br(**11**) | **8** | 42 | 6 | 6 |
| 8 | 4-Br(**11**) | **9** | 48 | 8 | ∼7 |
| 9 | 2-MeO(**12**) | **6** | 73 | 4 | 10 |
| 10 | 2-MeO(**12**) | **7** | 85 | rac | 12 |
| 11 | 2-MeO(**12**) | **8** | 97 | 2 | ∼14 |
| 12 | 2-MeO(**12**) | **9** | 90 | 5 | ∼13 |
| 13 | 4-MeO(**13**) | **6** | 70 | 10 | 10 |
| 14 | 4-MeO(**13**) | **7** | 75 | 10 | ∼11 |
| 15 | 4-MeO(**13**) | **8** | 63 | 2 | 9 |
| 16 | 4-MeO(**13**) | **9** | 75 | 12 | ∼11 |

*Note.* Reactions were performed by using trans-β-nitrostyrene derivative (0.2 mmol) and acetylacetone (0.4 mmol).
[a]Isolated yield.
[b]Enantiomeric excess was determined by HPLC analysis using YMC chiral ART Amylose-C column.[22]
[c]TON (Turnover number) = [moles of desired product (chiral secondary alcohol) formed]/[moles of catalyst used].
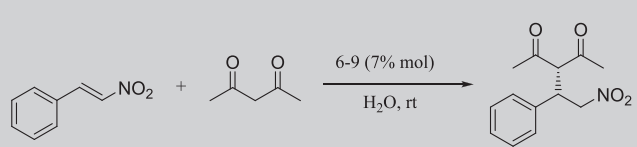
reaction solvents such as water, toluene, and dichloromethane by using the supporting material SBA-15 and mMCM-41. As shown in Table 6, no product formation was observed in the presence of those materials (entries 1–6). Then, bifunctional urea-amine organocatalysts **4** and **5**, and their silica supported counterparts **6–9** were examined in the same reactions. From Table 6, we can see that the solvent has clearly affected the catalytic performance of catalysts. In all entries, the product formation in water were yielded higher than those in dichloromethane or toluene. The highest conversion was obtained under the catalysis of **6** with poor enantioselectivity at room temperature (Table 6, entry 13).

Next, the effect of changes in the amount of catalyst and temperature on catalytic activity was investigated (Table 6, entries 14 and 15). Increasing the reaction temperature and the amount of catalyst gave lower conversion and enantioselectivity (Table 6, entries 14 and 15). After these results from the entries, the optimized conditions were preferred as follows: room temperature, 7% mol of catalyst and water as solvent.

Silica supported catalysts **6–9** gave moderate to high conversions with poor enantioselectivities for various substrates (Table 7). In case of electro-donating substituents at p- or o-positions of benzene ring, high conversions with low enantioselectivity were obtained in the presence of **6–9** (Table 7, entries 9–16). In contrast, electron-withdrawing substituents at p- or o-positions of benzene ring resulted in lower conversions and enantioselectivity (Table 7, entries 1–8).

To investigate the recyclability of **6–9**, the reaction between acetylacetone and β-nitrostyrene was studied under the optimized condition (Table 8). The recovery

**TABLE 8** Recycling studies of mesoporous silica-supported catalysts **6–9** in enantioselective Michael addition of acetylacetone to trans-β-nitrostyrene



| Entry | Run | Catalyst | Conversion (%)[a] | ee (%)[b] | TON[c] |
|---|---|---|---|---|---|
| **1** | 1 | **6** | 94 | 7 | 13 |
| **2** | 2 | **6** | 73 | 7 | 10 |
| **3** | 3 | **6** | 37 | 5 | 5 |
| **4** | 1 | **7** | 92 | 6 | 13 |
| **5** | 2 | **7** | 70 | 8 | 10 |
| **6** | 3 | **7** | 50 | 10 | 7 |
| **7** | 1 | **8** | 93 | 5 | 13 |
| **8** | 2 | **8** | 65 | 2 | 9 |
| **9** | 3 | **8** | 46 | 1 | ~6 |
| **10** | 1 | **9** | 97 | 3 | ~14 |
| **11** | 2 | **9** | 47 | 2 | ~6 |
| **12** | 3 | **9** | 34 | 2 | ~5 |

*Note.* Reactions were performed by using trans-β-nitrostyrene derivative (0.2 mmol) and acetylacetone (0.4 mmol).
[a]Isolated yield.
[b]Enantiomeric excess was determined by HPLC analysis using YMC chiral ART Amylose-C column.[22]
[c]TON (Turnover number) = [moles of desired product (chiral secondary alcohol) formed]/[moles of catalyst used].

**TABLE 9** Comparison of homogenous chiral catalyst **4** and heterogenous chiral solid catalyst **8** in ATH of acetophenone with previously reported chiral diamine derivative catalysts

| Entry | Cat. | S/C | Solvent | Time (h) | Conversion (%) | ee(%) | Ref. |
|---|---|---|---|---|---|---|---|
| **1**[a] | 4 | 250/1 | $^i$PrOH | 24 | 99 | _33_ | This work |
| **2**[a] | M-1 | 100/1 | $^i$PrOH | 24 | 81 | 89 | Zhou et al.[79] |
| **3**[a] | TsDPEN derivatives (8) | 100/1 | $^i$PrOH | 40 | 83 | 82 | Zhang et al.[80] |
| **4**[a] | Proline-DPEN | 100/1 | $HCO_2Na$ | 24 | 100 | 90 | Manville et al.[81] |
| **5**[a] | 3,3′,5,5′-TM-TsDPEN | 100/1 | $HCO_2Na$ | 24 | 99 | 89 | Liu et al.[82] |
| **6**[a] | N′-Me-TsDPEN | 100/1 | $HCO_2H/Et_3N$ | 10 | 99 | 96 | Martins et al.[83] |
| **7**[a] | Tethered-TsDPEN | 200/1 | $HCO_2H/Et_3N$ | 24 | 100 | 95 | Martins et al.[84] |
| **9**[b] | 8 | 125/1 | $^i$PrOH | 24 | 87 | 24 | This work |
| **10**[b] | TsDPEN@MCM-41 | 100/1 | $HCO_2H/Et_3N$ | 8 | 99 | 96 | Liu et al.[76] |
| **11**[b] | TsDPEN@SBA-15 | 100/1 | $HCO_2H/Et_3N$ | 8 | 99 | 96 | Liu et al.[76] |

[a]Homogenous enantioselective transfer hydrogenation.
[b]Heterogeneous enantioselective transfer hydrogenation.

of the catalysts **6–9** were performed as same as in ATH. According to the results in Table 8, all catalysts showed a gradual decrease in catalytic reactivity after the first run. FT-IR measurements of recovered **6–9** were taken to determine whether there was a change in the active site of catalysts. All the catalysts have the similar FT-IR spectra, but that spectrum was different from the FT-IR spectrum recorded before the first use in catalytic

reaction (see Supporting information for the spectra). It was found that some shifts in wavelengths of the characteristic peaks of catalysts **6–9** after the first run occurred in addition to the appearance of some new peaks. These observations for the recovered catalysts **6–9** can be probably due to the leaching of catalysts from mesoporous silica structures or the chemical instability of organic structure in reaction media. Therefore, the decrease in the catalytic activity of recovered catalysts **6–9** can be attributed to the instability of grafted **4** and **5** in channels of MSNs.[77]

### 3.2.3 | Comparison of the catalysts

Because the introduction of 1,2-diphenylethylenediamine as a chiral ligand for the Ru(II)-catalyzed asymmetric transfer hydrogenation of ketones, several ligands of this type have been reported.[78] Table 9 is summarized the comparison of the efficiency of solid chiral catalyst **8** and its homogenous counterpart **4** with previously reported catalysts in the obtained results for the enantioselective transfer hydrogenation of acetophenone. As shown, the catalysts synthesized in this work are as effective as other catalysts in terms of catalytic activity. But the results for the enantioselectivity in the case of **4** and **8** were obtained lower than the results of other catalysts.

## 4 | CONCLUSION

The synthesis of a series of mesoporous silica-grafted chiral urea-amine bifunctional catalysts **6–9** has been reported. The catalytic efficiencies of these synthesized catalysts in enantioselective transfer hydrogenation of aromatic ketones and enantioselective Michael addition of acetylacetone to nitroolefins were investigated. In enantioselective Michael addition of acetylacetone to nitroolefins, **6–9** showed remarkably high catalytic activity (up to 98%) but poor enantioselectivity. In ATH of aromatic ketones, chiral urea-amin catalysts **4** and **5** catalyzed the reactions to afford the corresponding alcohols in moderate to high conversion (31%–70%) with poor to moderate enantioselectivity (4%–38% *ee*). Under the optimized conditions, their silica supported derivatives **6–9** exhibited comparable enantioselectivity but lower catalytic activity. Increasing the S/C ratio resulted in high catalytic activity (95%) and better enantioselectivity (44% *ee*) compared with their homogeneous counterparts. In general, the mMCM-41 supported catalysts **8** and **9** showed higher catalytic activity than **6** and **7**. The different catalytic activities of **6–9** demonstrate that the structural morphology of mesoporous silica nanoparticles has important effect on performance of heterogeneous catalysts. Although the catalysts were losing their activities gradually in multiple runs, the easy preparation and recovery of the catalysts are the key advantages of this methodology. Further investigation to improve the efficiency and recyclability of these kind of catalysts is ongoing in our laboratory and will be published in due course.

### AUTHOR CONTRIBUTIONS
**Yaşar Gök:** Conceptualization; funding acquisition; investigation; methodology; project administration; supervision; visualization. **İrem Tutkum Aykut:** Investigation; methodology. **Halil Zeki GÖK:** Investigation; methodology.

### CONFLICT OF INTEREST
There is no conflict of interest between the authors.

### DATA AVAILABILITY STATEMENT
The data that support the findings of this study are available in the supplementary material of this article.

### ORCID
*Yaşar Gök* https://orcid.org/0000-0003-3134-7560
*Halil Zeki Gök* https://orcid.org/0000-0001-7641-2683

### REFERENCES
[1] H. J. Federsel, *Nat. Rev. Drug Discov.* **2005**, *4*, 685.
[2] K. M. Rentsch, *J. Biochem. Biophys. Methods* **2002**, *54*, 1.
[3] J. H. Kim, A. R. Scialli, *Toxicol. Sci.* **2011**, *122*(1), 1.
[4] R. J. D'Amato, M. S. Loughnan, E. Flynn, J. Folkman, *Proc. Natl. Acad. Sci. U. S. A.* **1994**, *91*, 4082.
[5] H. Sauer, J. Gunther, J. Hescheler, M. Wartenberg, *Am. J. Pathol.* **2000**, *156*, 151.
[6] E. Tokunaga, T. Yamamoto, E. Ito, N. Shibata, *Sci. Rep.* **2018**, *8*, 6.
[7] E. N. Jacobsen, A. Pfaltz, H. Yamamoto, *Comprehensive Asymmetric Catalysis*, Springer, Berlin **1999**.
[8] I. Ojima, *Catalytic Asymmetric Synthesis*, Second ed., Wiley, New York **2000**.
[9] T. P. Yoon, E. N. Jacobsen, *Science (80-.)* **2003**, *299*, 1691.

[10] T. Ohkuma, R. Noyori, in *Comprehensive Asymmetric Catalysis*, (Eds: E. N. Jacobsen, A. Pfaltz, H. Yamamoto) Vol. 1, Springer-Berlin **1999** Chapter 6.1.

[11] T. Ohkuma, M. Kitamura, R. Noyori, in *Catalytic Asymmetric Synthesis*, (Ed: I. Ojima), Wiley-VCH, New York **2000** Chapter 1.

[12] T. Ohkuma, R. Noyori, in *Transition Metals for Organic Synthesis: Building Blocks and Fine Chemicals*, (Eds: M. Beller, C. Bolm), Wiley-VCH, Weinheim, Germany **1998** 25.

[13] J. M. Brown, in *Comprehensive Asymmetric Catalysis*, (Eds: E. N. Jacobsen, A. Pfaltz, H. Yamamoto) Vol. 1, Springer-Berlin **1999** Chapter 5.1.

[14] J. M. Brown, *J. Organomet. Chem.* **2004**, *689*, 4006.

[15] J. Halpern, in *Asymmetric Synthesis*, (Ed: J. D. Morrison) Vol. 5, Academic Press, New York **1994** Chapter 1.

[16] M. Heitbaum, F. Glorius, I. Escher, *Angew. Chem., Int. Ed.* **2006**, *45*, 4732.

[17] J. Meng, F. Chang, Y. Su, R. Liu, T. Cheng, G. Liu, *ACS Catal.* **2019**, *9*, 8693.

[18] H. T. Chen, S. Huh, J. W. Wiench, M. Pruski, V. S. Y. Lin, *J. Am. Chem. Soc.* **2005**, *127*, 13305.

[19] S. Elavarasan, K. Kala, I. Muhammad, A. Bhaumik, M. Sasidharan, *Mol. Catal.* **2019**, *476*, 110521.

[20] P. Van Der Voort, K. Leus, E. De Canck, in *Introduction to Porous Materials*, (Eds: D. Atwood, B. Crabtree, G. Meyer, D. Woollins), Wiley, Cambridge **2019**.

[21] J. G. Croissant, Y. Fatieiev, A. Almalik, N. M. Khashab, *Adv. Healthcare Mater.* **2018**, *7*, 1700831.

[22] M. Nikoorazm, B. Tahmasbi, S. Gholami, P. Moradi, *Appl. Organomet. Chem.* **2020**, aoc.5919.

[23] M. Nikoorazm, Z. Rezaei, B. Tahmasbi, *J. Porous Mater.* **2020**, *27*, 671.

[24] A. Ghorbani-Choghamarani, B. Tahmasbi, R. H. E. Hudson, A. Heidari, *Microporous Mesoporous Mater.* **2019**, *284*, 366.

[25] M. Nikoorazm, A. Ghorbani-Choghamarani, A. Panahi, B. Tahmasbi, N. Noori, *J. Iran. Chem. Soc.* **2018**, *15*, 181.

[26] M. Nikoorazm, P. Moradi, N. Noori, *J. Porous Mater.* **2020**, *27*, 1159.

[27] P. Van Der Voort, D. Esquivel, E. De Canck, F. Goethals, I. Van Driessche, F. J. Romero-Salguero, *Chem. Soc. Rev.* **2013**, *42*, 3913.

[28] A. Ahadi, S. Rostamnia, P. Panahi, L. D. Wilson, Q. Kong, Z. An, M. Shokouhimehr, *Catalysts* **2019**, *9*, 9020140.

[29] W. Xie, H. Wang, *Renewable Energy* **2020**, *145*, 1709.

[30] W. Xie, Y. Han, H. Wang, *Renewable Energy* **2018**, *125*, 675.

[31] W. Xie, X. Zang, *Food Chem.* **2018**, *257*, 15.

[32] A. Ghorbani-Choghamarani, B. Tahmasbi, N. Noori, S. Faryadi, *C. R. Chim.* **2017**, *20*, 132.

[33] B. Atashkar, A. Rostami, H. Gholami, B. Tahmasbi, *Res. Chem. Intermed.* **2015**, *41*, 3675.

[34] L. Shiri, B. Tahmasbi, *Phosphorus, Sulfur Silicon Relat. Elem.* **2017**, *192*, 53.

[35] A. Hu, G. T. Yee, W. Lin, *J. Am. Chem. Soc.* **2005**, *127*, 12486.

[36] G. B. Heggannavar, C. G. Hiremath, D. D. Achari, V. G. Pangarkar, M. Y. Kariduraganavar, *ACS Omega* **2018**, *3*, 8017.

[37] K. Wu, D. Su, J. Liu, R. Saha, J. P. Wang, *Nanotechnology* **2019**, *30*, 502003.

[38] B. Shrestha, L. Tang, G. Romero, *Adv. Ther.* **2019**, *2*, 1900076.

[39] T. Sun, Y. S. Zhang, B. Pang, D. C. Hyun, M. Yang, Y. Xia, *Angew. Chem., Int. Ed.* **2014**, *53*, 12320.

[40] E. K. Lim, T. Kim, S. Paik, S. Haam, Y. M. Huh, K. Lee, *Chem. Rev.* **2015**, *115*, 327.

[41] T. Seki, K. McEleney, C. M. Crudden, *Chem. Commun.* **2012**, *48*, 6369.

[42] D. J. Mihalcik, W. Lin, *Angew. Chem., Int. Ed.* **2008**, *47*, 6229.

[43] J. Gao, J. Liu, S. Bai, P. Wang, H. Zhong, Q. Yang, C. Li, *J. Mater. Chem.* **2009**, *19*, 8580.

[44] K. Berijani, H. Hosseini-Monfared, *Inorg. Chim. Acta* **2018**, *471*, 113.

[45] H. Li, M. Pérez-Trujillo, X. Cattoën, R. Pleixats, *ACS Sustainable Chem. Eng.* **2019**, *7*, 14815.

[46] G. Szllsi, *Catal. Sci. Technol.* **2018**, *8*, 389.

[47] F. Meemken, A. Baiker, *Chem. Rev.* **2017**, *117*, 11522.

[48] T. Yasukawa, H. Miyamura, S. Kobayashi, *Chem. Soc. Rev.* **2014**, *43*, 1450.

[49] Q. L. Zhou, *Privileged Chiral Ligands and Catalysts*, Wiley **2011**.

[50] S. Gladiali, E. Alberico, *Chem. Soc. Rev.* **2006**, *35*, 226.

[51] J. Cossy, F. Eustache, P. I. Dalko, *Tetrahedron Lett.* **2001**, *42*, 5005.

[52] J. Takehara, S. Hashiguchi, A. Fujii, S. I. Inoue, T. Ikariya, R. Noyori, *Chem. Commun.* **1996**, *12*, 233.

[53] P. G. Echeverria, C. Férard, P. Phansavath, V. Ratovelomanana-Vidal, *Cat. Com.* **2015**, *62*, 95.

[54] X. Wu, D. Vinci, T. Ikariya, J. Xiao, *Chem. Commun.* **2005**, 4447.

[55] D. D. Perrin, W. F. L. Armarego, *Purification of Laboratory Chemicals*, Second ed., Pergamon, Oxford, UK **1989**.

[56] D. Zhao, Q. Huo, J. Feng, B. F. Chmelka, G. D. Stucky, *J. Am. Chem. Soc.* **1998**, *120*, 6024.

[57] L. Shen, P. E. Laibinis, T. Alan Hatton, *Langmuir* **1999**, *15*, 447.

[58] A. Benvidi, M. Nikmanesh, M. Dehghan Tezerjani, S. Jahanbani, M. Abdollahi, A. Akbari, A. Rezaeipoor-Anari, *J. Electroanal. Chem.* **2017**, *787*, 145.

[59] W. Yao, J. Zhu, X. Zhou, R. Jiang, P. Wang, W. Chen, *Tetrahedron* **2018**, *74*, 4205.

[60] H. Zhao, H. Han, *J. Solid State Chem.* **2020**, *282*, 121074.

[61] L. B. de Oliveira Freitas, I. J. G. Bravo, W. A. de Almeida Macedo, E. M. de Sousa, *J. sol-Gel Sci. Technol.* **2016**, *77*, 186.

[62] A. Hakiki, B. Boukoussa, H. Habib, R. Hamacha, H. Hadj, F. Bekkar, F. Bettahar, A. P. Nunes-beltrao, S. Hacini, A. Bengueddach, *Mater. Chem. Phys.* **2018**, *212*, 415.

[63] S. Abaeezadeh, D. Elhamifar, M. Norouzi, M. Shaker, *Appl. Organomet. Chem.* **2019**, *33*, 1.

[64] W. Xie, L. Zhao, *Energy Convers. Manage.* **2014**, *79*, 34.

[65] A. M. Kaczmarek, S. Abednatanzi, D. Esquivel, C. Krishnaraj, H. S. Jena, G. Wang, K. Leus, R. Van Deun, F. J. Romero-Salguero, P. Van Der Voort, *Microporous Mesoporous Mater.* **2020**, *291*, 109687.

[66] K. S. W. Sing, *Pure Appl. Chem.* **1985**, *57*, 603.

[67] S. Rohani, G. Mohammadi Ziarani, A. Badiei, A. Ziarati, M. Jafari, A. Shayesteh, *Appl. Organomet. Chem.* **2018**, *32*, 4397.

[68] T. A. Arica, E. Ayas, M. Y. Arica, *Microporous Mesoporous Mater.* **2017**, *243*, 164.

[69] L. Zhang, J. Liu, J. Yang, Q. Yang, C. Li, *Chem.-An Asian J.* **2008**, *3*, 1842.

[70] C. P. Jaroniec, R. K. Gilpin, M. Jaroniec, *J. Phys. Chem. B* **1997**, *101*, 6861.

[71] X. Liu, P. Wang, Y. Yang, P. Wang, Q. Yang, *Chem.-An Asian J.* **2010**, *5*, 1232.

[72] X. Liu, P. Wang, L. Zhang, J. Yang, C. Li, Q. Yang, *Chem.-A Eur. J.* **2010**, *16*, 12727.

[73] D. Jiang, Q. Yang, H. Wang, G. Zhu, J. Yang, C. Li, *J. Catal.* **2006**, *239*, 65.

[74] S. Hashiguchi, A. Fujii, J. Takehara, T. Ikariya, R. Noyori, *J. Am. Chem. Soc.* **1995**, *117*, 7562.

[75] A. Fujii, S. Hashiguchi, N. Uematsu, T. Ikariya, R. Noyori, *J. Am. Chem. Soc.* **1996**, *118*, 2521.

[76] P. N. Liu, P. M. Gu, F. Wang, Y. Q. Tu, *Org. Lett.* **2004**, *6*, 169.

[77] Z. Tang, J. Sun, H. Zhao, S. Bai, X. Wu, H. Panezai, *Microporous Mesoporous Mater.* **2018**, *260*, 245.

[78] F. Foubelo, C. Nájera, M. Yus, *Tetrahedr. Asymm.* **2015**, *26*, 769.

[79] X. Zhou, X. Wu, B. Yang, J. Xiao, *J. Mol. Catal. A: Chem.* **2012**, *357*, 133.

[80] B. Zhang, H. Wang, G. Q. Lin, M. H. Xu, *Eur. J. Org. Chem.* **2011**, 4205.

[81] C. V. Manville, G. Docherty, R. Padda, M. Wills, *Eur. J. Org. Chem.* **2011**, 6893.

[82] J. Liu, Y. Wu, X. Li, A. S. C. Chan, *J. Organomet. Chem.* **2008**, *693*, 2177.

[83] J. E. D. Martins, M. A. Contreras Redondo, M. Wills, *Tetrahedr. Asymm.* **2010**, *21*, 2258.

[84] J. E. D. Martins, D. J. Morris, B. Tripathi, M. Wills, *J. Organomet. Chem.* **2008**, *693*, 3527.

## SUPPORTING INFORMATION

Additional supporting information may be found online in the Supporting Information section at the end of this article.